LAWRENCE
LIVERMORE
NATIONAL
LABORATORY

LLNL-TR-763689

Data Evaluation of Actinide Cross Sections: 240Am, 241Am, and 242Am

W. E. Ormand, S. Quaglioni, E. Jurgenson, M. A. Descalle, I. J. Thompson, J. E. Escher, W. Younes, C. M. Mattoon, B. Beck, J. T. Burke, T. Bailey

December 6, 2018

Disclaimer

This work performed under the auspices of the U.S. Department of Energy by Lawrence Livermore National Laboratory under Contract DE-AC52-07NA27344.

Data Evaluation of Actinide Cross Sections: ^{240}Am, ^{241}Am, and ^{242}Am
LLNL-TR-763689

W. E. Ormand,[1,*] S. Quaglioni,[1] E. Jurgenson,[1] M. A. Descalle,[1] I. J. Thompson,[1]
J. E. Escher,[1] W. Younes,[1] C. M. Mattoon,[1] B. Beck,[1] J. T. Burke,[1] and T. Bailey[1]

[1] *Lawrence Livermore National Laboratory, P.O. Box 808, L-414, Livermore, California 94551, USA*

(Dated: December 20, 2018)

Evaluations for neutron-induced reactions on the isotopes ^{240}Am, ^{241}Am, and ^{242}Am were performed by optimizing reaction-model calculations based on existing experimental data from both direct measurements and surrogate reactions. The evaluated data were based on results obtained form the LLNL reaction codes YAHFC and FRESCO using up-to-date nuclear models; including an improvement upon some previous treatments for inelastic processes. Nuclear reaction codes generated data for all relevant reaction channels, which were then translated into Generalized Nuclear Data Structure and LLNL's Evaluated Neutron Data Libraries (ENDL). These data libraries were tested for potential errors and applied to verification and validation (V&V) tests suites where applicable for comparisons.

I. INTRODUCTION

This report documents the recent evaluation of the ^{240}Am, ^{241}Am, and ^{242}Am cross section sets. Nuclear data evaluation is the fundamental interface that transforms experimentally measured nuclear cross section data and into a continuous curves and data libraries that are: 1) consistent with other measurements and nuclear reaction theory/models, and 2) required by down-stream users. All experiments that generate nuclear data need to include an evaluation step for their data to be broadly useful to the end users.

In the research performed here, several neutron-induced nuclear reaction cross sections have been evaluated. These evaluations were then processed into a form suitable for end user codes, and the processed data underwent the verification and validation (V&V) step. Finally, the "experimental" data libraries (ENDL2011.N-ex1 and EDL2011.N-ex2) were released for internal use within LLNL. This work made use of the unique capabilities that exist at LLNL in the Nuclear & Particle Physics and Nuclear Data & Theory groups and leveraged existing NNSA/Defense Program investments in reaction modeling codes, processing codes, and the V&V suites. The end-product is updated libraries that include the latest measurements of key cross sections.

The steps performed to create the evaluation, processing, validation and verification, and library release are described in the following sections. For completeness, the appendices contain all the parameters used in the evaluation for the ^{240}Am, ^{241}Am and ^{242}Am cross sections.

II. EXPERIMENTAL DATA

Experimental data for the $^{240-242}$Am isotopes are primarily limited to direct measurements of (n,γ), (n,f), and $(n,2n)$ for ^{241}Am and experimental data for indirect (surrogate) reactions for (n,f) on all three isotopes. Most of the experimental data can be found in the Experimental Nuclear Reaction Data (EXFOR) database (version 2018-09-11) maintained by the U.S. Nuclear Data Program (USNDP) at Brookhaven National Laboratory (http://www.nndc.bnl.gov/exfor/exfor.htm).

A. ^{240}Am Data

For ^{240}Am, experimental data is available for only the (n,f) channel via recent surrogate experiments. [1, 2].

B. ^{241}Am Data

For ^{241}Am, extensive experimental data exists for the (n,γ), (n,f) and $(n,2n)$ channels.

* ormand1@llnl.gov

C. ^{242}Am Data

For ^{242}Am, experimental data is available for only the (n, f) channel via recent surrogate experiments.

III. MODELING

A full evaluation requires consistent data tabulated in a data library for each incident neutron energy. The required data consist of cross sections for each channel, energy spectra for all emitted particles (including photons), angular distributions for emitted particles, average number of neutrons, $\bar{\nu}$, emitted during fission, and the prompt fission neutron spectrum. Consistency in the cross sections requires that the cross sections for the channels sum to the total reaction cross section. This consistency requirement generally means that an evaluated data library is obtained from a model calculation where parameters in the model are selected to reproduce existing experimental data. It must be stated that often different experimental data sets are inconsistent, and sometimes violate physical reality. Consequently, expert judgement is must be applied during the modeling process. In this work, the evaluation was performed within the Hauser-Feshbach framework extended to include additional physics concepts.

It should be noted that overall, Hauser-Feshbach modeling is dependent on a fairly large number of parameters that define the internal models describing the various aspects of the reaction process. The starting point for the Hauser-Feshbach process in the optical potential, which effectively defines the total and elastic cross sections, as well as direct inelastic processes via coupled channels along the low-lying rotational band. Other inelastic reactions exciting states just above the rotational band and generally in the continuum density of states can be accounted for by both a distorted-wave Born approximation (DWBA) for other direct processes and a pre-equilibrium model less direct processes where the incident neutron is captured but emitted prior to achieving statistical equilibrium. Once statistical equilibrium is achieved particle emission and fission are accounted for within the Hauser-Feshbach formalism. For the most part, this modeling process has limited predictive capability, and most of the parameters are determined to reproduce experimental data. Towrads this end, since some model parameters cannot be determined from Am isotopes alone, we made extensive use of behaviors exhibited in other actinide nuclei, e.g., ^{234,235,238}U and ^{239}Pu to provide guidance.

Here, the reaction modeling was performed using the LLNL developed Hauser-Feshbach reaction system YAHFC [3]. YAHFC is a Monte Carlo based computer code that tracking the entire reaction process on an event-by-event basis. It offers new features compared to older codes, and has a simple user interface. YAHFC is coupled to the optical model computer code FRESCO [4] to compute transmission coefficients, direct excitations within the ground-state rotational band, and inelastic excitations in the DWBA framework.

A. Optical Potential

In this work, we primarily utilize the actinide optical potential developed by Soukhovitskii [5]. Substantial effort has gone into this potential, which does an excellent job reproducing experimental data for the total cross section for most of the major actinides. Overall, it must be noted that the optical potential is primarily fit to the total cross section (with uncertainties of just a few percent) and inelastic transitions in the rotational band of ^{238}U at low energies (below the onset of fission). In general, experimental data for the elastic cross section and other inelastic processes is lacking. Overall, the magnitude of the elastic cross section has a fairly large uncertainty as derived from experimental data. However, it is fairly well constrained at approximately the five percent level based on the physical features of the potential.

1. Coupled Channels

Direct inelastic processes (that is the incident neutron is not captured) were accounted for in two ways. First, direct excitations to states within the ground rotational band were accounted for within the standard coupled-channels framework. The second is described below in Section III B describing the DWBA process. The coupled channels approach is described in the FRESCO manual [4]. The levels coupled to the ground state are listed in Table I while the deformation parameters are given in Table II.

TABLE I. List of excited states utilized in the coupled-channels calculation for each target nucleus.

^{240}Am		^{241}Am		^{242}Am	
E_x	J^π	E_x	J^π	E_x	J^π
0.0000	3^-	0.0000	$\frac{5}{2}^-$	0.0000	1^-
0.0410	4^-	0.4120	$\frac{7}{2}^-$	0.0441	0^-
0.0960	5^-	0.9370	$\frac{9}{2}^-$	0.0527	3^-
0.1580	6^-	0.1575	$\frac{11}{2}^-$	0.0758	2^-
0.2330	7^-	0.2337	$\frac{13}{2}^-$	0.1480	5^-
0.3160	8^-	0.2390	$\frac{15}{2}^-$	0.2630	6^-
		0.4182	$\frac{17}{2}^-$	0.2631	7^-
		0.5256	$\frac{19}{2}^-$		

TABLE II. List of deformation parameters used in the coupled-channels calculation for each target nucleus.

	^{240}Am	^{241}Am	^{242}Am
β_2	0.223	0.223	0.224
β_4	0.095	0.087	0.079
β_6	-0.019	-0.022	-0.026

B. Inelastic excitations via DWBA

Previous studies of neutron-induced reactions on actinide targets note that inelastic reactions for incident neutron energies $\geq$ 8 MeV are under predicted by standard reaction modeling processes, namely direct, pre-equilibirium, and compound. A strong signature for this deficiency is provided by the neutron emission spectrum for ^{238}U(n, Xn) reactions for an incident neutron energy of 14 MeV. As in the previous ENDF/B-VII evaluation for ^{238}U, we accounted for this additional inelastic process within the framework the distorted-wave Born approximation (DWBA) with a set of excited states with a well defined aligned angular momentum K coupled to the ground state. These DWBA states, are not coupled to the rotational band, and do not alter the direct excitation of the ground-state band, or alter the total reaction cross section. Overall, these states are not representative of known discrete states within the spectrum. Instead, they represent sates generally embedded within the continuum and thus are given excitations energies matching the energy grid of the calculation. This is different from the ENDF/B-VII library where the DWBA states are treated as discrete states and are labeled as an inelastic transition to a discrete state even though these inserted states do not have a gamma-decay patch. Here, the DWBA states are treated as a set of states embedded into the continuum energy spectrum. Once excited, they are decayed in the same manner as any other continuum energy bin in the statistical decay process of the Hauser-Feshbach formalism. The DWBA states included in each calculation are based on previous evaluation for ^{238}U [6] and extended to the Am isotopes whose ground state has non-zero K. These states are given in Table III. Note that the states are defined by an explicit K value and have a final angular momentum and parity value that arises due to coupling with the ground-state angular momentum and parity.

TABLE III: List of DWBA states utilized in the calculations for each target nucleus. The K value of the state and the coupled angular momentum are given.

^{240}Am				^{241}Am				^{242}Am			
E_x	J^π	K	β_K	E_x	J^π	K	β_K	E_x	J^π	K	β_K
0.9972	3^+	3	9.00E-02	0.9950	$\frac{5}{2}^+$	3	9.00E-02	0.9972	1^+	3	9.00E-02
0.9972	4^+	3	9.00E-02	0.9950	$\frac{7}{2}^+$	3	9.00E-02	0.9972	2^+	3	9.00E-02
0.9972	5^+	3	9.00E-02	0.9950	$\frac{9}{2}^+$	3	9.00E-02	0.9972	3^+	3	9.00E-02
0.9972	6^+	3	9.00E-02	0.9950	$\frac{11}{2}^+$	3	9.00E-02	0.9972	4^+	3	9.00E-02
1.0603	3^-	2	5.00E-02	1.0900	$\frac{5}{2}^-$	2	5.00E-02	1.0603	1^-	2	5.00E-02
1.0603	4^-	2	5.00E-02	1.0900	$\frac{7}{2}^-$	2	5.00E-02	1.0603	2^-	2	5.00E-02
1.0603	5^-	2	5.00E-02	1.0900	$\frac{9}{2}^-$	2	5.00E-02	1.0603	3^-	2	5.00E-02
1.1500	3^+	3	8.50E-02	1.1500	$\frac{5}{2}^+$	3	8.50E-02	1.1500	1^+	3	8.50E-02
1.1500	4^+	3	8.50E-02	1.1500	$\frac{7}{2}^+$	3	8.50E-02	1.1500	2^+	3	8.50E-02

TABLE III: Continued

^{240}Am				^{241}Am				^{242}Am			
E_x	J^π	K	β_K	E_x	J^π	K	β_K	E_x	J^π	K	β_K
1.1500	5^+	3	8.50E-02	1.1500	$\frac{9}{2}^+$	3	8.50E-02	1.1500	3^+	3	8.50E-02
1.1500	6^+	3	8.50E-02	1.1500	$\frac{11}{2}^+$	3	8.50E-02	1.1500	4^+	3	8.50E-02
1.1500	3^-	2	5.00E-02	1.1500	$\frac{5}{2}^-$	2	5.00E-02	1.1500	1^-	2	5.00E-02
1.1500	4^-	2	5.00E-02	1.1500	$\frac{7}{2}^-$	2	5.00E-02	1.1500	2^-	2	5.00E-02
1.1500	5^-	2	5.00E-02	1.1500	$\frac{9}{2}^-$	2	5.00E-02	1.1500	3^-	2	5.00E-02
1.2500	3^+	3	4.00E-02	1.2500	$\frac{5}{2}^+$	3	4.00E-02	1.2500	1^+	3	4.00E-02
1.2500	4^+	3	4.00E-02	1.2500	$\frac{7}{2}^+$	3	4.00E-02	1.2500	2^+	3	4.00E-02
1.2500	5^+	3	4.00E-02	1.2500	$\frac{9}{2}^+$	3	4.00E-02	1.2500	3^+	3	4.00E-02
1.2500	6^+	3	4.00E-02	1.2500	$\frac{11}{2}^+$	3	4.00E-02	1.2500	4^+	3	4.00E-02
1.3500	3^+	3	3.20E-02	1.3500	$\frac{5}{2}^+$	3	3.20E-02	1.3500	1^+	3	3.20E-02
1.3500	4^+	3	3.20E-02	1.3500	$\frac{7}{2}^+$	3	3.20E-02	1.3500	2^+	3	3.20E-02
1.3500	5^+	3	3.20E-02	1.3500	$\frac{9}{2}^+$	3	3.20E-02	1.3500	3^+	3	3.20E-02
1.3500	6^+	3	3.20E-02	1.3500	$\frac{11}{2}^+$	3	3.20E-02	1.3500	4^+	3	3.20E-02
1.4500	3^+	3	3.20E-02	1.4500	$\frac{5}{2}^+$	3	3.20E-02	1.4500	1^+	3	3.20E-02
1.4500	4^+	3	3.20E-02	1.4500	$\frac{7}{2}^+$	3	3.20E-02	1.4500	2^+	3	3.20E-02
1.4500	5^+	3	3.20E-02	1.4500	$\frac{9}{2}^+$	3	3.20E-02	1.4500	3^+	3	3.20E-02
1.4500	6^+	3	3.20E-02	1.4500	$\frac{11}{2}^+$	3	3.20E-02	1.4500	4^+	3	3.20E-02
1.5500	3^+	3	3.20E-02	1.5500	$\frac{5}{2}^+$	3	3.20E-02	1.5500	1^+	3	3.20E-02
1.5500	4^+	3	3.20E-02	1.5500	$\frac{7}{2}^+$	3	3.20E-02	1.5500	2^+	3	3.20E-02
1.5500	5^+	3	3.20E-02	1.5500	$\frac{9}{2}^+$	3	3.20E-02	1.5500	3^+	3	3.20E-02
1.5500	6^+	3	3.20E-02	1.5500	$\frac{11}{2}^+$	3	3.20E-02	1.5500	4^+	3	3.20E-02
1.6500	3^+	3	3.20E-02	1.6500	$\frac{5}{2}^+$	3	3.20E-02	1.6500	1^+	3	3.20E-02
1.6500	4^+	3	3.20E-02	1.6500	$\frac{7}{2}^+$	3	3.20E-02	1.6500	2^+	3	3.20E-02
1.6500	5^+	3	3.20E-02	1.6500	$\frac{9}{2}^+$	3	3.20E-02	1.6500	3^+	3	3.20E-02
1.6500	6^+	3	3.20E-02	1.6500	$\frac{11}{2}^+$	3	3.20E-02	1.6500	4^+	3	3.20E-02
1.7500	3^+	3	3.20E-02	1.7500	$\frac{5}{2}^+$	3	3.20E-02	1.7500	1^+	3	3.20E-02
1.7500	4^+	3	3.20E-02	1.7500	$\frac{7}{2}^+$	3	3.20E-02	1.7500	2^+	3	3.20E-02
1.7500	5^+	3	3.20E-02	1.7500	$\frac{9}{2}^+$	3	3.20E-02	1.7500	3^+	3	3.20E-02
1.7500	6^+	3	3.20E-02	1.7500	$\frac{11}{2}^+$	3	3.20E-02	1.7500	4^+	3	3.20E-02
1.8500	3^+	3	3.10E-02	1.8500	$\frac{5}{2}^+$	3	3.10E-02	1.8500	1^+	3	3.20E-02
1.8500	4^+	3	3.10E-02	1.8500	$\frac{7}{2}^+$	3	3.10E-02	1.8500	2^+	3	3.20E-02
1.8500	5^+	3	3.10E-02	1.8500	$\frac{9}{2}^+$	3	3.10E-02	1.8500	3^+	3	3.20E-02
1.8500	6^+	3	3.10E-02	1.8500	$\frac{11}{2}^+$	3	3.10E-02	1.8500	4^+	3	3.20E-02
1.9500	3^-	4	2.10E-02	1.9500	$\frac{5}{2}^-$	4	2.10E-02	1.9500	1^-	4	2.10E-02
1.9500	4^-	4	2.10E-02	1.9500	$\frac{7}{2}^-$	4	2.10E-02	1.9500	2^-	4	2.10E-02
1.9500	5^-	4	2.10E-02	1.9500	$\frac{9}{2}^-$	4	2.10E-02	1.9500	3^-	4	2.10E-02
1.9500	6^-	4	2.10E-02	1.9500	$\frac{11}{2}^-$	4	2.10E-02	1.9500	4^-	4	2.10E-02
1.9500	7^-	4	2.10E-02	1.9500	$\frac{13}{2}^-$	4	2.10E-02	1.9500	5^-	4	2.10E-02
1.9500	3^-	2	2.90E-02	1.9500	$\frac{5}{2}^-$	2	2.90E-02	1.9500	1^-	2	2.90E-02
1.9500	4^-	2	2.90E-02	1.9500	$\frac{7}{2}^-$	2	2.90E-02	1.9500	2^-	2	2.90E-02
1.9500	5^-	2	2.90E-02	1.9500	$\frac{9}{2}^-$	2	2.90E-02	1.9500	3^-	2	2.90E-02
2.0500	3^-	2	2.90E-02	2.0500	$\frac{5}{2}^-$	2	2.90E-02	2.0500	1^-	2	2.90E-02
2.0500	4^-	2	2.90E-02	2.0500	$\frac{7}{2}^-$	2	2.90E-02	2.0500	2^-	2	2.90E-02
2.0500	5^-	2	2.90E-02	2.0500	$\frac{9}{2}^-$	2	2.90E-02	2.0500	3^-	2	2.90E-02
2.1500	3^-	2	2.90E-02	2.1500	$\frac{5}{2}^-$	2	2.90E-02	2.1500	1^-	2	2.90E-02
2.1500	4^-	2	2.90E-02	2.1500	$\frac{7}{2}^-$	2	2.90E-02	2.1500	2^-	2	2.90E-02
2.1500	5^-	2	2.90E-02	2.1500	$\frac{9}{2}^-$	2	2.90E-02	2.1500	3^-	2	2.90E-02
2.2500	3^-	2	2.70E-02	2.2500	$\frac{5}{2}^-$	2	2.70E-02	2.2500	1^-	2	2.70E-02
2.2500	4^-	2	2.70E-02	2.2500	$\frac{7}{2}^-$	2	2.70E-02	2.2500	2^-	2	2.70E-02
2.2500	5^-	2	2.70E-02	2.2500	$\frac{9}{2}^-$	2	2.70E-02	2.2500	3^-	2	2.70E-02
2.3500	3^-	2	2.50E-02	2.3500	$\frac{5}{2}^-$	2	2.60E-02	2.3500	1^-	2	2.50E-02
2.3500	4^-	2	2.50E-02	2.3500	$\frac{7}{2}^-$	2	2.60E-02	2.3500	2^-	2	2.50E-02
2.3500	5^-	2	2.50E-02	2.3500	$\frac{9}{2}^-$	2	2.60E-02	2.3500	3^-	2	2.50E-02

TABLE III: Continued

^{240}Am				^{241}Am				^{242}Am			
E_x	J^π	K	β_K	E_x	J^π	K	β_K	E_x	J^π	K	β_K
2.4500	3^-	2	2.40E-02	2.4500	$\frac{5}{2}^-$	2	2.40E-02	2.4500	1^-	2	2.40E-02
2.4500	4^-	2	2.40E-02	2.4500	$\frac{7}{2}^-$	2	2.40E-02	2.4500	2^-	2	2.40E-02
2.4500	5^-	2	2.40E-02	2.4500	$\frac{9}{2}^-$	2	2.40E-02	2.4500	3^-	2	2.40E-02
2.5500	3^-	2	2.30E-02	2.5500	$\frac{5}{2}^-$	2	2.30E-02	2.5500	1^-	2	2.30E-02
2.5500	4^-	2	2.30E-02	2.5500	$\frac{7}{2}^-$	2	2.30E-02	2.5500	2^-	2	2.30E-02
2.5500	5^-	2	2.30E-02	2.5500	$\frac{9}{2}^-$	2	2.30E-02	2.5500	3^-	2	2.30E-02
2.6500	3^-	2	2.20E-02	2.6500	$\frac{5}{2}^-$	2	2.20E-02	2.6500	1^-	2	2.20E-02
2.6500	4^-	2	2.20E-02	2.6500	$\frac{7}{2}^-$	2	2.20E-02	2.6500	2^-	2	2.20E-02
2.6500	5^-	2	2.20E-02	2.6500	$\frac{9}{2}^-$	2	2.20E-02	2.6500	3^-	2	2.20E-02
2.7500	3^-	2	2.10E-02	2.7500	$\frac{5}{2}^-$	2	2.10E-02	2.7500	1^-	2	2.10E-02
2.7500	4^-	2	2.10E-02	2.7500	$\frac{7}{2}^-$	2	2.10E-02	2.7500	2^-	2	2.10E-02
2.7500	5^-	2	2.10E-02	2.7500	$\frac{9}{2}^-$	2	2.10E-02	2.7500	3^-	2	2.10E-02
2.8500	3^-	2	2.00E-02	2.8500	$\frac{5}{2}^-$	2	2.00E-02	2.8500	1^-	2	2.00E-02
2.8500	4^-	2	2.00E-02	2.8500	$\frac{7}{2}^-$	2	2.00E-02	2.8500	2^-	2	2.00E-02
2.8500	5^-	2	2.00E-02	2.8500	$\frac{9}{2}^-$	2	2.00E-02	2.8500	3^-	2	2.00E-02
2.9500	3^-	2	1.90E-02	2.9500	$\frac{5}{2}^-$	2	1.90E-02	2.9500	1^-	2	1.90E-02
2.9500	4^-	2	1.90E-02	2.9500	$\frac{7}{2}^-$	2	1.90E-02	2.9500	2^-	2	1.90E-02
2.9500	5^-	2	1.90E-02	2.9500	$\frac{9}{2}^-$	2	1.90E-02	2.9500	3^-	2	1.90E-02
3.0500	3^-	2	1.80E-02	3.0500	$\frac{5}{2}^-$	2	1.80E-02	3.0500	1^-	2	1.80E-02
3.0500	4^-	2	1.80E-02	3.0500	$\frac{7}{2}^-$	2	1.80E-02	3.0500	2^-	2	1.80E-02
3.0500	5^-	2	1.80E-02	3.0500	$\frac{9}{2}^-$	2	1.80E-02	3.0500	3^-	2	1.80E-02
3.1500	3^-	2	1.70E-02	3.1500	$\frac{5}{2}^-$	2	1.70E-02	3.1500	1^-	2	1.70E-02
3.1500	4^-	2	1.70E-02	3.1500	$\frac{7}{2}^-$	2	1.70E-02	3.1500	2^-	2	1.70E-02
3.1500	5^-	2	1.70E-02	3.1500	$\frac{9}{2}^-$	2	1.70E-02	3.1500	3^-	2	1.70E-02
3.2500	3^-	2	1.60E-02	3.2500	$\frac{5}{2}^-$	2	1.60E-02	3.2500	1^-	2	1.60E-02
3.2500	4^-	2	1.60E-02	3.2500	$\frac{7}{2}^-$	2	1.60E-02	3.2500	2^-	2	1.60E-02
3.2500	5^-	2	1.60E-02	3.2500	$\frac{9}{2}^-$	2	1.60E-02	3.2500	3^-	2	1.60E-02
3.3500	3^-	2	1.50E-02	3.3500	$\frac{5}{2}^-$	2	1.50E-02	3.3500	1^-	2	1.50E-02
3.3500	4^-	2	1.50E-02	3.3500	$\frac{7}{2}^-$	2	1.50E-02	3.3500	2^-	2	1.50E-02
3.3500	5^-	2	1.50E-02	3.3500	$\frac{9}{2}^-$	2	1.50E-02	3.3500	3^-	2	1.50E-02

The overall impact of the DWBA states on the neutron emission spectrum is illustrated for ^{238}U, which was used to guide the Am calculations, in Figure 1. The contributions from elastic, direct coupled channels, pre-equilibrium, compound, and fission to the (n, Xn) emission spectrum are shown. In this calculation, similar DWBA states were utilized as listed in Table III with the exception that since the ground state is $J = 0$ only a single DWBA state is included, and are represented by the orange line. The black circles are the experimental data from Ref. [8]. The magenta line represents inelastic processes from the coupled-channels calculation for the rotational band, while the grey line is from pre-equilibrium emission. The large peak $\sim$ 14 MeV is from elastic scattering. The green line is the sum of processes from the Hauser-Feshbach calculation, while the blue line is the contribution from fission obtained from the FREYA code [9]. Finally, the red line is the sum of all neutron emission processes. The impact of the DWBA states is to fill in the neutron emission spectrum between 11-13 MeV. Overall, without the DWBA states, it is not possible to account for the emission spectrum in a realistic way that is consistent with data. The DWBA states used here for the Am-isotopes are similar to those used for the ^{238}U ENDF/B-VII evaluation.

C. Pre-equilibrium Emission and elastic scattering

The primary components of an incident neutron reaction are elastic, direct inelastic (via coupled channels), and capture reactions. The latter of these makes up the brunt of the reaction, and is the essence of the statistical Hauser-Feshbach process. This final stage requires that the captured neutron dissipate its energy into the target, thereby creating the well-known compound nucleus. At higher incident neutron energies, the time scale for the neutron to dissipate its energy is of the order, or shorter, than the time scale for the neutron to be emitted. Thus, leading to what is referred to as pre-equilibirum emission. Here, we used the two-component exciton model of Koning and

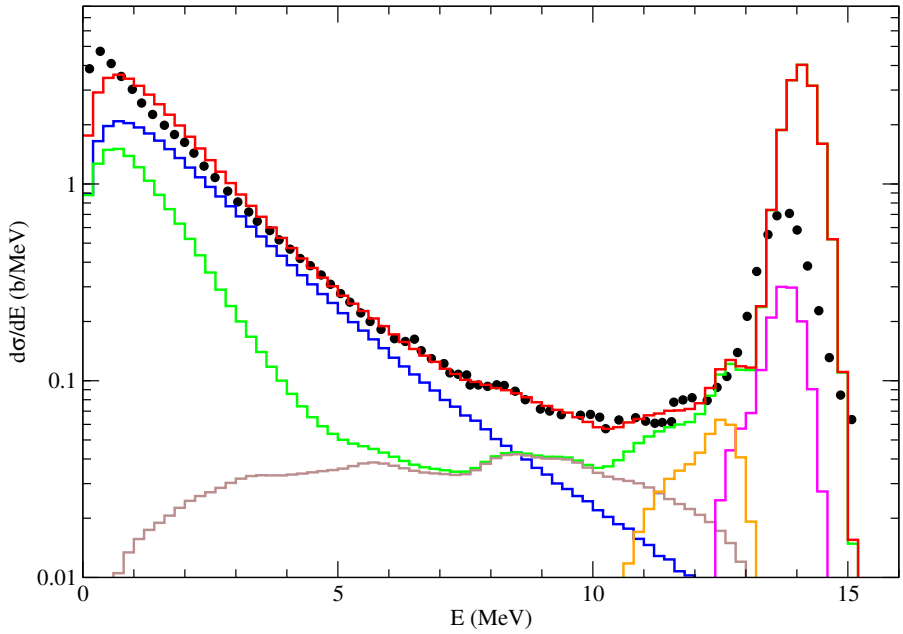

FIG. 1. Contributions to the neutron emission spectrum for all channels ^{238}U(n, Xn) for E_n-14.1 MeV. The black circles are from experiment, while the red line represents to the sum of all components in a theoretical calculation. The blue line is from fission, while grey is pre-equilibrium emission, magenta represent inelastic processes from the coupled-channels calculation for the rotational band, and orange is inelastic scattering from the DWBA states. The large peak at ∼14 MeV is from elastic scattering.

Duijvestijn [7]. Overall, the (n, Xn) emission spectrum gives guidance for the pre-equilibrium parameters as well. Some additional constraint could be obtained from the $(n, 2n)$ cross section. On the whole, however, this was found to be quite difficult as the calculations tended to over-predict the $(n, 2n)$ cross section in for 8 MeV $\leq E_n \leq$ 13 MeV, as shown in Figure 2 with the blue line. The symbols with error bars represent experimental data tabluated in the EXFOR data base. In principle, it is possible to decrease the $(n, 2n)$ cross section with the pre-equilibrium model by "hardening" the emission spectrum, i.e., the emission of higher energy neutrons. However, "hardening" the emission spectrum shifts the cross section into the (n, n') channel, which then affects the (n, Xn) spectrum in the 11-14 MeV range. In addition, "hardening" pre-equilibrium tends to shift cross section from the $(n, 3n)$ channel, which then leads to an increase in the $(n, 2n)$ cross section for $E_n > 15$ MeV. In short, it is not possible to adequately model the ^{238}U$(n, 2n)$ cross section within the models and parameters used here.

The resolution of this issue seems to lie in the details of the optical potential. As mentioned above the optical potential is primarily determined by fitting a set of parameters to the total cross section and inelastic reactions within the coupled channels framework. The elastic cross section is composed of two components: 1) shape elastic, which is a property of the optical potential, and 2) compound, which is the remission of an absorbed neutron back to the original target state. The shape elastic cross section is determined by features of the optical potential, and overall there is very little experimental data, and what little there is have uncertainties of 10% or more. We found that the issue regarding the $(n, 2n)$ cross section could be resolved with by increasing the elastic cross section by approximately 5% for higher values of E_n. This would point to a need to refit the optical potential, which is an exercise beyond what was viable here. Instead, we opted for an "engineering" fix by scaling the optical potential and then renormalizing the transmission coefficients to reduce the absorption cross section. This was achieved here by scaling the elastic cross section by

$$\sigma_{\rm Elastic} = \sigma^{\rm OP}_{\rm Elastic}[1 + S(1 - \exp(-bE_n))], \tag{1}$$

where $\sigma^{\rm OP}_{\rm Elastic}$ is the elastic cross section from the optical potential, $S = 0.05$ is the scale factor, and $b = 0.5$ is a factor introduced to provide an energy dependence to the scaling factor. With the values here, the elastic cross section is unaltered at low incident neutron energies, and is increased by 5% at high energy.

Finally, since the total cross section is well reproduced by the Soukhovitskii potential, the transmission coefficients, T_{lj}, which govern the absorption cross section, for each channel with orbital angular momentum l coupled to angular momentum j are reduced by

$$T_{lj} = T^{\rm OP}_{lj}[1 - S(1 - \exp(-bE_n))], \tag{2}$$

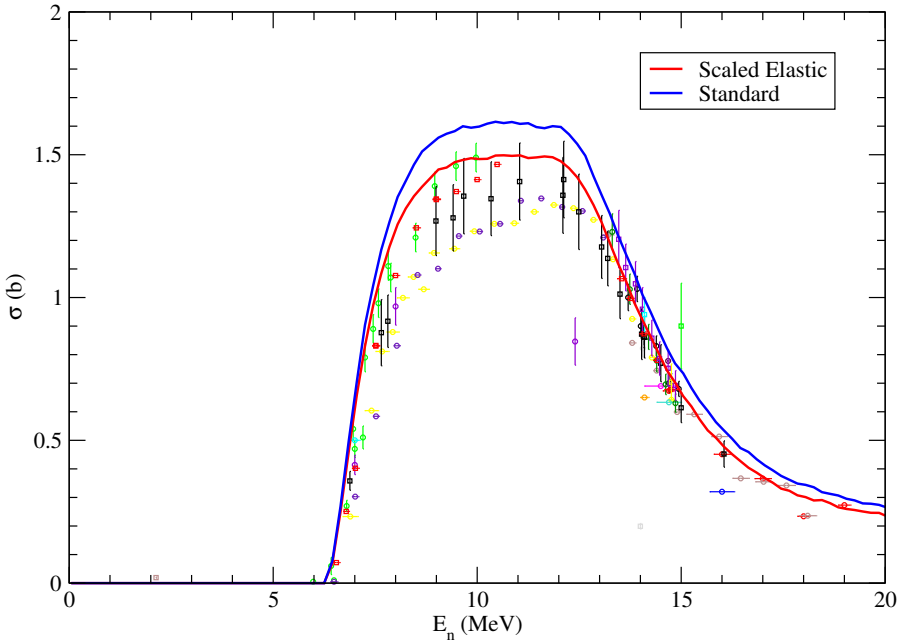

FIG. 2. Calculations of the ^{238}U$(n, 2n)$ cross section in comparison with experimental data (from the EXFOR data base) for a standard Hauser-Feshbach calculation with pre-equilibrium (blue line) and a Hauser-Feshbach calculation where the elastic cross section was enhanced by 5% (red line) as given by Eq. 1.

where again the superscript OP denotes the optical potential value. The affect of rescaling the elastic cross section on the ^{238}U$(n, 2n)$ cross section is seen in Figure 2 with the red line.

Given that similar high-quality data doesn't exist for the Am isotopes, the calculations performed here were assumed to be affected by the same physics models for ^{238}U.

D. Hauser-Feshbach parameters

Here, we tabulate the principal parameters used to define the models used within the calculation. The parameters defined here have the same context and meaning as in the TALYS code and manual [10] and are given in Table IV for the level density and the fission model (for two barriers denoted with the subscript B_i).

The electro-magnetic (EM) strength functions were modeled using standard approaches. In particular, the electric-dipole ($E1$) strength function had the form postulated by Kopecky and Uhl [11] with up to three Lorentzians, each with centroid E_i, width Γ_i, and strength S_i. For ^{242}Am, a third Lorentzian with $E_3 = 5.0$ MeV, $\Gamma_3 = 5.0$ MeV, $S_3 = 1.365$ mb was added in order to reproduce the evaluated $l = 0$ gamma-width $\Gamma_\gamma(l = 0) = 46 \pm 3$ meV. The strength functions for the remain modes, $E2$, $E3$, $M1$, and $M2$, were modeled with a single Lorentzian with the parameters listed in Table IV.

TABLE IV: List of Hauser-Feshbach model parameters used for each nucleus.

Parameter	^{239}Am	^{240}Am	^{241}Am	^{242}Am	^{243}Am
Level Density					
a	13.795	13.840	13.885	13.931	13.976
Δ	0.500	0.000	0.700	0.000	0.626
E_{Shell}	1.572	0.210	0.271	0.264	1.884
γ	0.0763	0.0762	0.0761	0.0760	0.0759
E_{Match}	3.737	1.507	3.490	1.865	3.516
Fission					
Barrier#1					
E_{B_1}	5.90	6.70	6.90	6.45	6.20
$\hbar\omega_{B_1}$	0.60	0.50	0.70	0.50	0.50
a_{B_1}	13.794	13.840	13.885	13.931	13.976
Δ_{B_1}	0.800	0.000	0.120	0.050	0.200

TABLE IV: Continued

Parameter	^{239}Am	^{240}Am	^{241}Am	^{242}Am	^{243}Am
E_{Shell,B_1}	1.572	2.500	2.600	2.500	2.000
γ_{B_1}	0.0760	0.0760	0.0760	0.0760	0.0760
E_{Match,B_1}	3.100	3.500	2.700	3.100	2.500
Barrier#2					
E_{B_2}	5.90	6.00	6.20	5.70	5.800
$\hbar\omega_{B_2}$	0.60	0.60	0.80	0.60	0.600
a_{B_2}	13.794	13.840	13.885	13.931	13.976
Δ_{B_2}	0.500	0.000	0.000	0.000	0.250
E_{Shell,B_2}	2.000	2.500	2.700	3.600	2.200
γ_{B_2}	0.0760	0.0760	0.0760	0.0760	0.0760
E_{Match,B_2}	3.200	3.000	3.500	3.300	2.50
EM Strength					
$E1$					
E_1 (MeV)	11.28	11.28	11.28	11.28	11.28
Γ_1 (MeV)	2.48	2.48	2.48	2.48	2.48
S_1 (mb)	325	325	325	325	325
E_2 (MeV)	13.73	13.73	13.73	13.73	13.73
Γ_2 (MeV)	4.25	4.25	4.25	4.25	4.25
S_2 (mb)	384	384	384	384	384
E_3 (MeV)	-	-	-	5	-
Γ_3 (MeV)	-	-	-	5	-
S_3 (mb)	-	-	-	1.4	-
$E2$					
E_1 (MeV)	10.152	10.138	10.123	10.109	10.096
Γ_1 (MeV)	3.242	3.230	3.218	3.206	3.194
S_1 (mb)	0.637	0.638	0.638	0.639	0.640
$E3$					
E_1 (MeV)	10.152	10.138	10.123	10.109	10.096
Γ_1 (MeV)	3.242	3.230	3.218	3.206	3.194
S_1 (mb)	5.1×10^{-4}	5.1×10^{-4}	5.1×10^{-4}	5.1×10^{-4}	5.1×10^{-4}
$M1$					
E_1 (MeV)	6.607	6.597	6.588	6.579	6.570
Γ_1 (MeV)	4.000	4.000	4.000	4.000	4.000
S_1 (mb)	1.852	1.848	1.525	1.522	1.519
$M2$					
E_1 (MeV)	6.607	6.597	6.588	6.579	6.570
Γ_1 (MeV)	4.000	4.000	4.000	4.000	4.000
S_1 (mb)	1.48×10^{-3}	1.48×10^{-3}	1.22×10^{-3}	1.22×10^{-3}	1.22×10^{-3}

IV. RESULTS

A. ^{241}Am Results

We begin with the results for ^{241}Am, which generally has more experimental data to constrain theoretical calculations. An important consideration is that the same parameters were used to define the fission models across the entire $^{240-242}$Am isotopic chain. For example, second-chance fission for $^{241}\mathrm{Am}(n,f)$ involves fission of the ^{241}Amcompound nucleus (following the emission of a neutron), which, in turn, is the system defining first-chance fission for the $^{240}\mathrm{Am}(n,f)$ reaction. Thus, the model parameters were not constrained by a single system, but rather across the chain in order to achieve consistent agreement between experiment and modeling. The "fits" to experimental data were conducted through observation, rather than with a stringent least-squares minimization procedure. This was primarily due to the complexity of and the non-uniqueness of the parameters in the fission models, and difficulties in "fitting" data across the isotopic chain. For the most part, the experimental uncertainties in the fission cross sections are fairly large as well, and there is little difference in the quality of the "fits".

In addition to the direct and surrogate data for the ^{241}Am fission cross section, fission parameters for second-chance fission were strongly influenced by the $^{241}\mathrm{Am}(n,2n)$ cross section, which is measured with excellent precision. Given

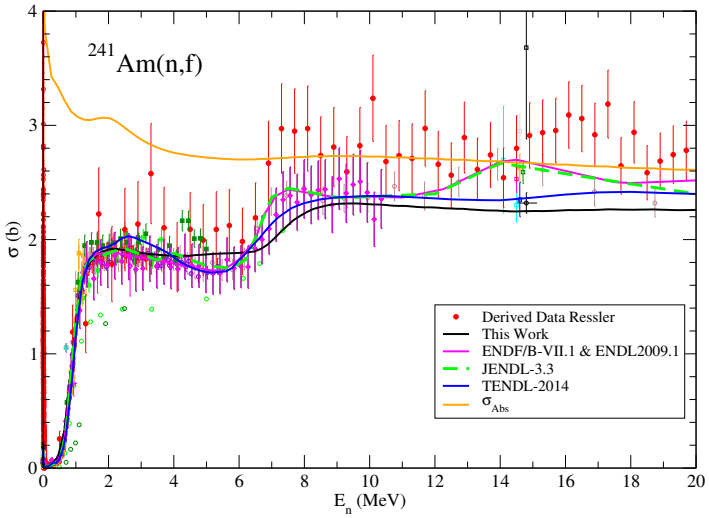

FIG. 3. Comparison of results from this evaluation for the $^{241}\mathrm{Am}(n,f)$ cross section (black line) with experimental data in EXFOR and the indirect data of Ressler. Values for previous evaluations in the libraries ENDF/B-VII.1, JENDL-3.3, and TENDL-2014 are shown.

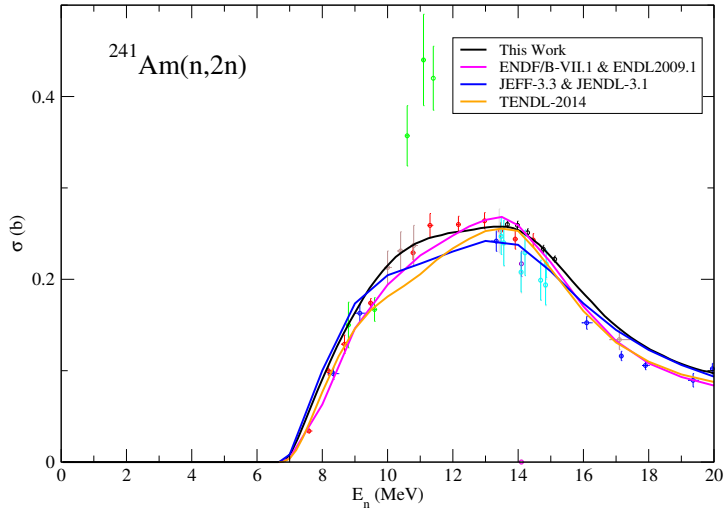

FIG. 4. Comparison of results from this evaluation for the $^{241}\mathrm{Am}(n,2n)$ cross section (black line) with experimental data in EXFOR and values for previous evaluations in other libraries, ENDF/B-VII.1, JENDL-3.3, and TENDL-2014, are shown.

that for $E_n \approx 10-15$ MeV, the (n,f), (n,n'), and $(n,2n)$ cross section must sum to the absorption cross section, σ_{Abs} (defined here as the sum of compound and pre-equilibrium cross sections), and the (n,n') is guided by knowledge from ^{238}U as described above, the $(n,2n)$ cross section provides a strong constraint/guidance regarding the maximum value the ^{241}Am cross section can have in this region. In Figure 3, we show the results of the current evaluation in comparison with experimental data compiled in EXFOR and the indirect data of Ressler as well as with previous evaluations in other libraries. The current evaluation for the $^{241}\mathrm{Am}(n,2n)$ cross section is shown in Figure 4 in comparison with data compiled in EXFOR and earlier evaluations. Regarding the indirect measurement (derived from a surrogate reaction), the total absorption cross section is shown with the solid orange line. This represents an upper bound to reaction processes, and it is clear that the derived data are inconsistent with this limit, and were not given any weight in determining the fission parameters.

Shown in Figure 5 are the principal channels for $^{241}\mathrm{Am}(n,X)$ reactions.

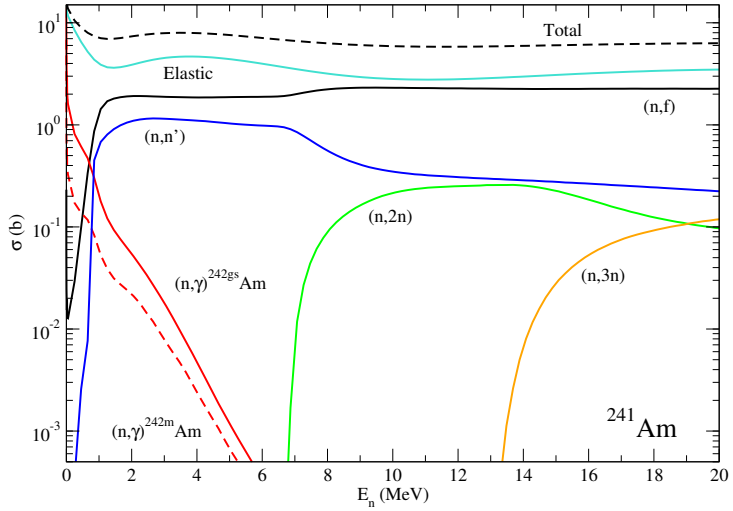

FIG. 5. Plot of the principal channels for $^{241}\mathrm{Am}(n, X)$ reactions.

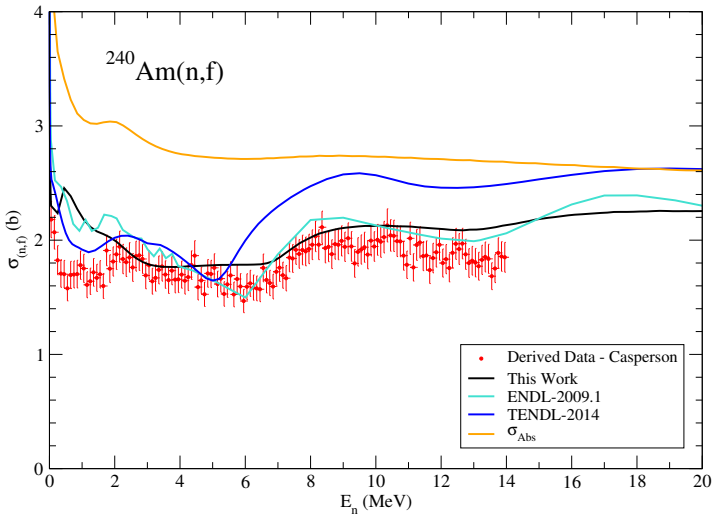

FIG. 6. Comparison of results from this evaluation for the $^{240}\mathrm{Am}(n, f)$ cross section (black line) with experimental data in EXFOR and the indirect data of Ressler. Values for previous evaluations in the libraries ENL-2009.1 and TENDL-2014 are shown. The absorption cross section is represented by the solid orange line.

B. ^{240}Am Results

The current evaluation for the $^{240}\mathrm{Am}(n, f)$ reaction (black line) is shown in Figure 6 in comparison with the derived data from Casperson and previous evaluations in the ENL-2009.1 and TENDL-2014 libraries. The total absorption cross section is also shown as the solid orange line. Agreement with the Casperson data is reasonable, except for $E_n < 2$ MeV. Past experience, however, points to the fact the surrogate technique breaks down for low energies. The Casperson data also influenced the $^{241}\mathrm{Am}(n, f)$ evaluation, where, as is seen in Figure 3, the evaluation tends to be larger than the central data points for $E_n \approx 4 - 6$ MeV, and smaller for $E_n \approx 6 - 7$ MeV. Overall, in order to achieve better agreement with the $^{240}\mathrm{Am}(n, f)$ data, it was necessary to increase the contribution due to first-chance in $^{241}\mathrm{Am}(n, f)$. Otherwise, the relative fission probability for the ^{241}Am compound (first-chance) in $^{240}\mathrm{Am}(n, f)$ is too large, which would lead to a substantial over estimate of the $^{240}\mathrm{Am}(n, f)$ cross section for $E_n \leq 4$ MeV.

Shown in Figure 7 are the principal channels for $^{240}\mathrm{Am}(n, X)$ reactions.

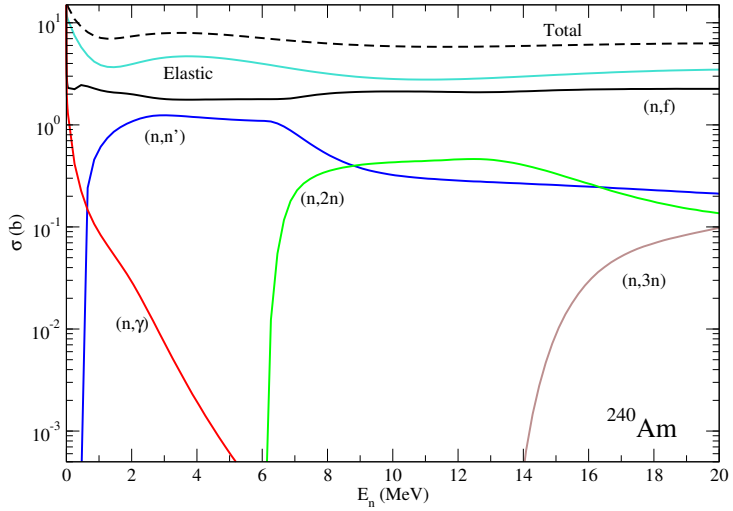

FIG. 7. Plot of the principal channels for Am240(n, X) reactions.

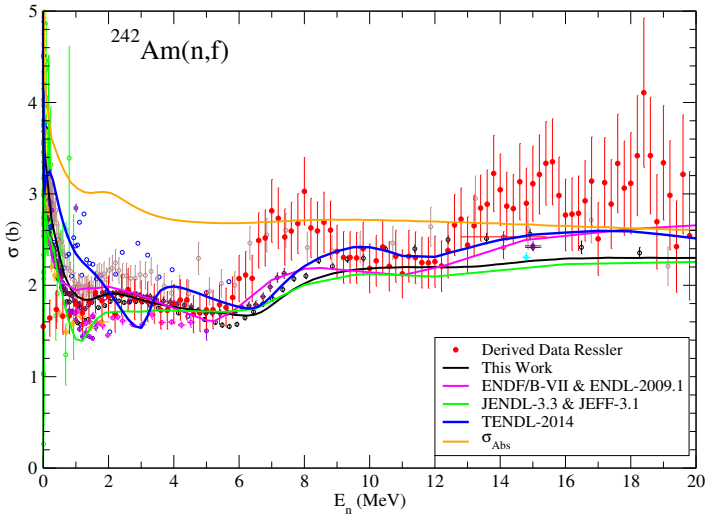

FIG. 8. Comparison of results from this evaluation for the ^{242}Am(n, f) cross section (black line) with experimental data in EXFOR and the indirect data of Ressler. Values for previous evaluations in the libraries ENDF/B-VII.1, JENDL-3.3, and TENDL-2014 are shown.

C. ^{242}Am Results

The current evaluation for the ^{242}Am(n, f) reaction (black line) is shown in Figure 8 in comparison with experimental data from compiled in the EXFOR and the derived data from Ressler. Previous evaluations in the ENDF/B-VII (also ENDL-2009.1), JENDL-3.3, and TENDL-2014 libraries. The total absorption cross section is also shown as the solid orange line.

Shown in Figure 9 are the principal channels for ^{242}Am(n, X) reactions.

V. DATA PROCESSING AND RELEASE PROCEDURES FOR NUCLEAR EVALUATIONS

The Hauser-Feshbach modeling provided files conatining the cross sections and angular distributions of outgoing neutrons and gamma rays for both the case when residual nuclei are in specific final states and when the residual nuclear states are unspecified. Exit channels that involve other charged particles - protons, deuterons, tritons, helions (^{3}He), and alphas, - were not included due to their extremely low cross section, and relative unimportance.

The evaluations produced from the YAHFC code are in ascii text tables of a form closely related to that produced by

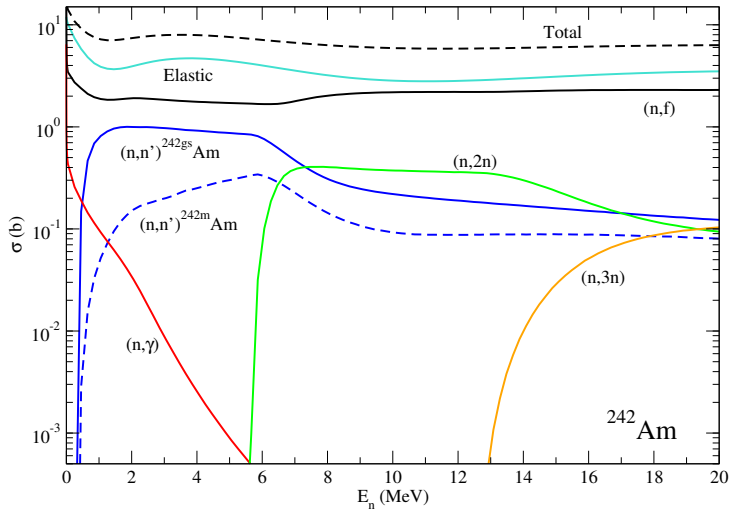

FIG. 9. Plot of the principal channels for $^{242}\mathrm{Am}(n, X)$ reactions.

the TALYS code, but in a more compact format. For example, a single outgoing product energy-angle distribution is contained in a single file instead of TALYS' single file for each angle and energy, greatly reducing the number of files one must manage. With no existing parser for this output, we opted to develop a new one that would translate to a native GNDS file and leverage existing capability to translate the GNDS file to LLNL's legacy library format, ENDL. The Generalized Nuclear Data Structure (GNDS) is the new next-generation international nuclear data format standard being developed at LLNL. Thus we produce the deliverable simultaneously in both the legacy and next-generation formats.

The output from YAHFC, however, is not fully sufficient for application use, and has to be supplemented by further information for low-energy reactions, and for specifying the products of fission reactions. Low-energy reactions of neutrons (below about 1 to 10 keV) are dominated by resonances, and these have to be specifically measured by time-of-flight neutron experiments. Similarly, the products of fission processes (prompt neutron multiplicities, prompt neutron energy distributions, total fission energy production, fission product distributions) were not fitted by the evaluator. In the present work for Americium isotopes, the resonance data and fission product data were adopted unchanged from the previous evaluations in the ENDL2009.3 library and subsequently from ENDF/B-VII.0. Note that the existing ENDL2009.3 evaluation for ^{240}Am was generated at LLNL in 2009 from TALYS calculations and the fission properties were transplanted from the existing ^{242}Am evaluation. One advantage to translating into GNDS is the ease of splicing in the parts of a full evaluation that YAHFC cannot produce.

To provide these new evaluations for testing, we followed current standard procedure at Livermore and created an experimental nuclear data library based on a full release library, in this case ENDL2009.3. Such an experimental library contains all the nuclides in the full release with only the new evaluations substituted in. This experimental release, called ENDL2009.3-ex5, is hosted in our developmental data directory at LLNL. All data in ENDL libraries is processed for deterministic and Monte Carlo simulations using the multigroup codes NDFGEN and MCFGEN, respectively. These also process cross sections that have been broadened by Maxwellian distributions to a range of temperatures suitable for applications. The new evaluations were then tested by comparing results from the 'ex' evaluations with those from the ENDL2009.3 library, among others, as detailed in the next section.

VI. VERIFICATION AND VALIDATION TESTING

The new evaluations for ^{240}Am, ^{241}Am, and ^{242}Am were processed and merged in ENDL2009.3-ex5mcf, the Monte Carlo library file. They were then tested using the Nuclear Data Group Automated Verification and Validation test suite [12]. The verification step consists of a 'Broomstick' test and the validation step relies on comparison to reaction ratio benchmark data.

The 'Broomstick' test consists of a thin cylinder of material made of a single isotope of density 1.0 g/cm^3. The cylinder is 105 cm long with a radius of 10^5 cm, long enough to be considered semi-infinite so that all incident neutrons interact once in the material, and thin enough to ensure once-scattered and secondary particles escape without interactions. A monoenergetic pencil beam of 1 or 14 MeV neutrons is directed along the cylinder axis. Currently, available tallies include the number of reactions per reaction type within the cylinder and leakage spectra

TABLE V. Sources of ^{240,241,242}Am evaluations in nuclear data libraries

	ENDF/B-VIII.0	ENDL2009.3	ENDL2009.3-ex5
^{240}Am	ENDF/B-VII.1	Younes (TALYS)	This Work
^{241}Am	New (Kawano)	ENDF/B-VII.0	This Work
^{242}Am	ENDF/B-VII.1	ENDF/B-VII.1	This Work

as a function of energy or angular emission.

Mercury simulations were run on Livermore Computing (LC) systems for the three Americium isotopes [13, 14]. Results were compared to those obtained with ENDL2009.3, ENDF/B-VII.1 and ENDF/B-VIII.0, three officially-released cross section libraries. The sources of the ^{240}Am, ^{241}Am, and ^{242}Amevaluations are summarized in Table V [6, 15]. Several differences were observed between the new evaluations and those in the released libraries.

Compared to ENDL2009.3, ^{240,241,242}Am contributions from the (n, n') channels were smaller at 1 MeV. 241Am showed an increase in (n, el) and a decrease in (n, f) reactions, while ^{240}Am and ^{242}Am exhibit an increase in (n, f) reactions.

At 14 MeV, the 3 new evaluations showed a decrease in (n, f) reactions and an increase in (n, el) reactions. ^{240,241}Am contributions from the (n, n') channels were stronger. Figure 9 indicates stronger ^{240}Am and ^{241}Am contributions from the $(n, 3n)$ channel and a decrease in $(n, 2n)$ reactions. These differences observed in the weaker channels were consistent with the initial model developed for ENDL2009.3-ex5 evaluations.

Contributions from the ^{240}Am(n, n') and (n, γ) channels at 1 MeV and $(n, 2n)$ channels at 14 MeV are now closer to those given by the ENDF/B released libraries, and contributions from the ^{241}Am(n, n') and (n, γ) channels at 1 MeV are now closer to those given by the new ENDF/B-VIII.0 released library for the simulations using the ENDL2009.3-ex5 library (see Figure 10).

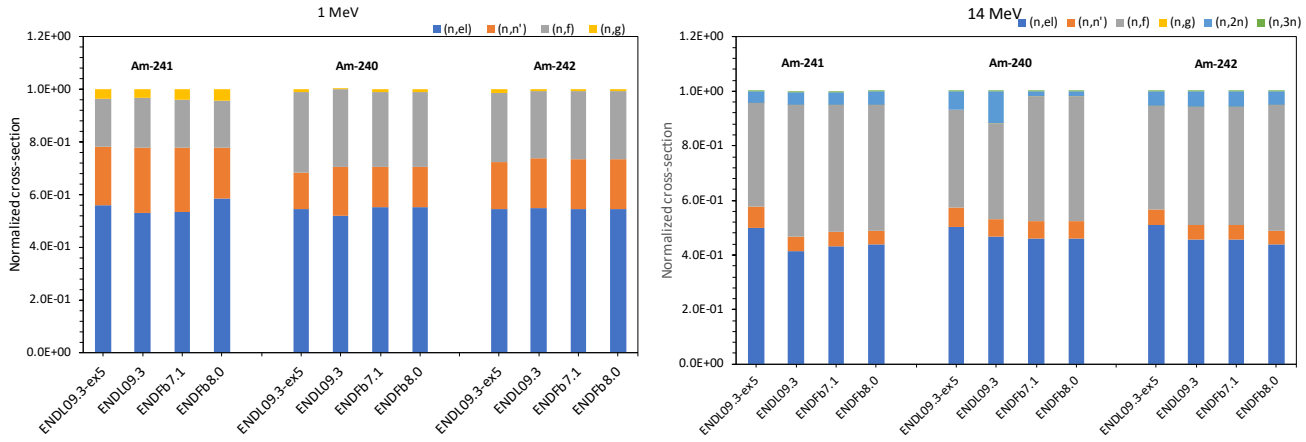

FIG. 10. Normalized summed cross-section contributions obtained from Mercury simulations for 1 MeV (left) and 14 MeV (right) neutrons incident on a thin cylinder of ^{240}Am, ^{241}Am, and ^{242}Am. Results are shown for the new Americium evaluations in ENDL2009.3-ex5, and existing evaluations in ENDL2009.3, ENDF/B-VII.1 and ENDF/B-VIII.0 cross-section libraries.

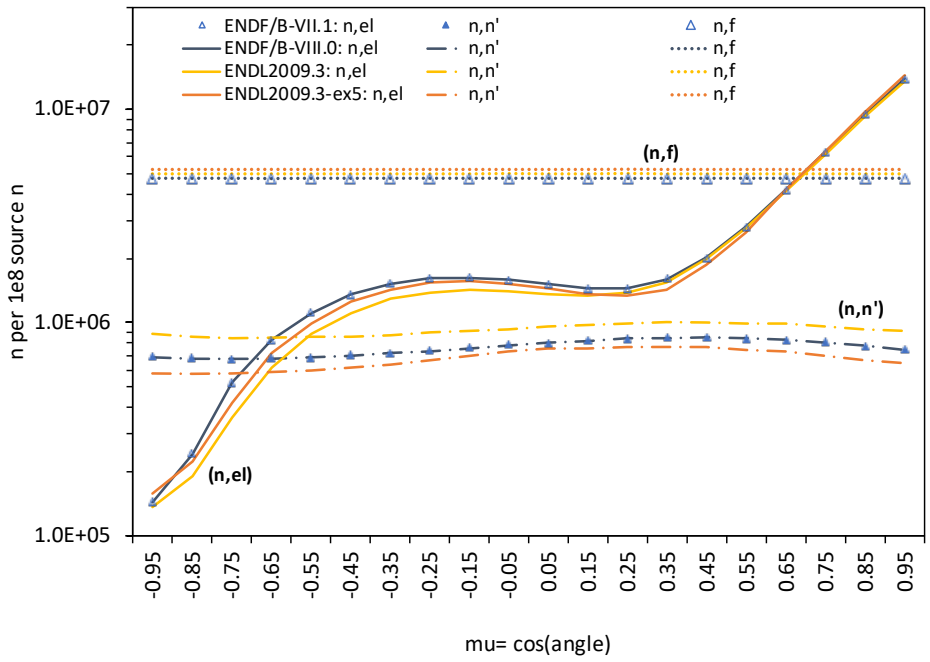

FIG. 11. Simulated angular distribution of outgoing neutrons following a single (n, el) reaction (full line), (n, n') reaction (dot-dashed line), and (n, f) reaction (dotted line) for 1 MeV neutrons incident on ^{240}Am for ENDL2009.3-ex5 (orange). Also shown are the corresponding distributions for ENDF/B-VIII.0 (black), END2009.3 (yellow) and ENDF/B-VII.1 (triangle).

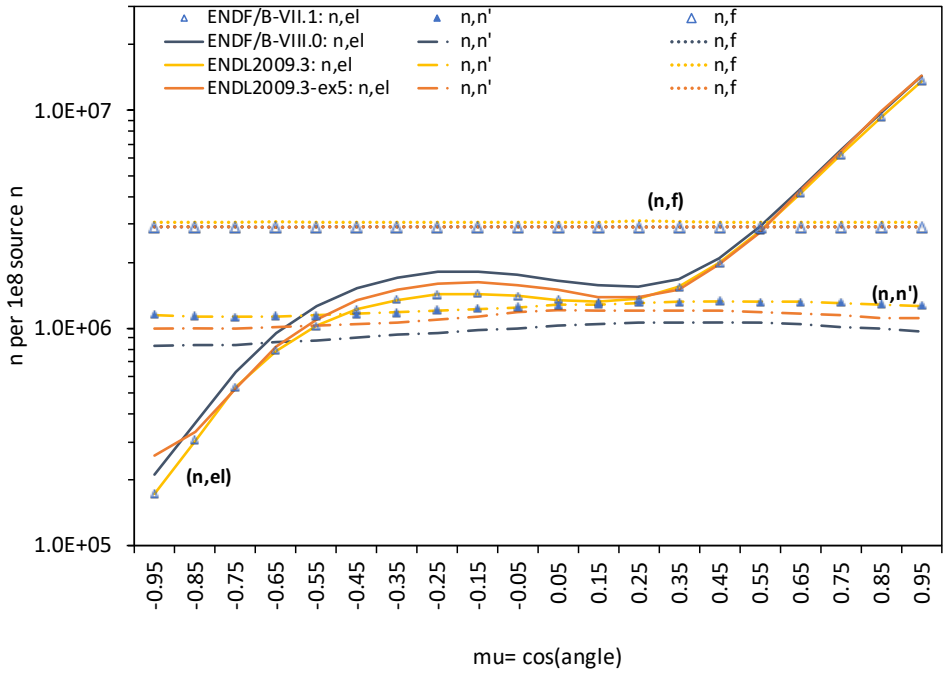

FIG. 12. Simulated angular distribution of outgoing neutrons following a single (n, el) reaction (full line), (n, n')reaction (dot-dashed line), and (n, f) reaction (dotted line) for 1 MeV neutrons incident on ^{241}Am for ENDL2009.3-ex5 (orange). Also shown are the corresponding distributions for ENDF/B-VIII.0 (black), END2009.3 (yellow) and ENDF/B-VII.1 (triangle).

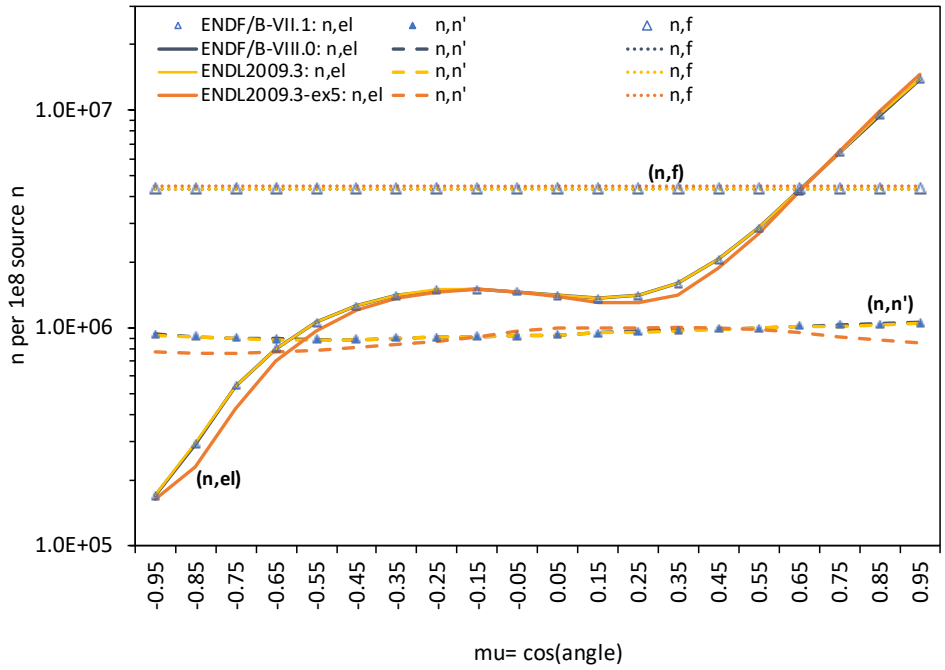

FIG. 13. Simulated angular distribution of outgoing neutrons following a single (n, el) reaction (full line), (n, n') reaction (dot-dashed line), and (n, f) reaction (dotted line) for 1 MeV neutrons incident on ^{242}Am for ENDL2009.3-ex5 (orange). Also shown are the corresponding distributions for ENDF/B-VIII.0 (black), END2009.3 (yellow) and ENDF/B-VII.1 (triangle).

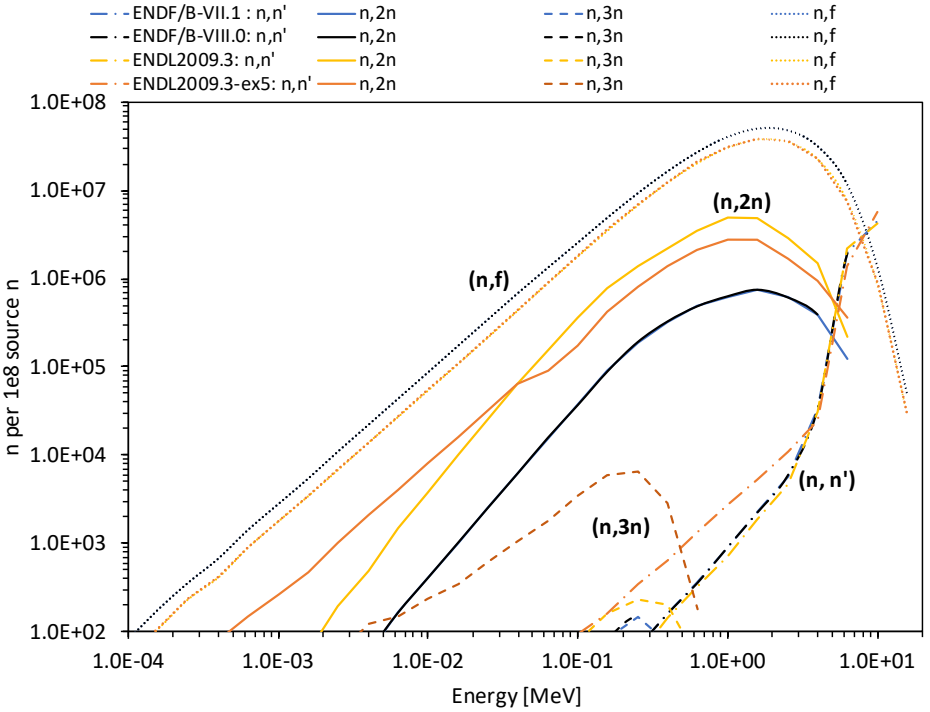

FIG. 14. Simulated energy distribution of outgoing neutrons following a single (n, n') reaction (dot-dashed line), $(n, 2n)$ reaction (full line), $(n, 3n)$ reaction (dashed line) and (n, f) reaction (dotted line) for 14 MeV neutrons incident on ^{240}Am for ENDL2009.3-ex5 (orange). Also shown are the corresponding distributions for ENDF/B-VIII.0 (black), END2009.3 (yellow) and ENDF/B-VII.1 (blue).

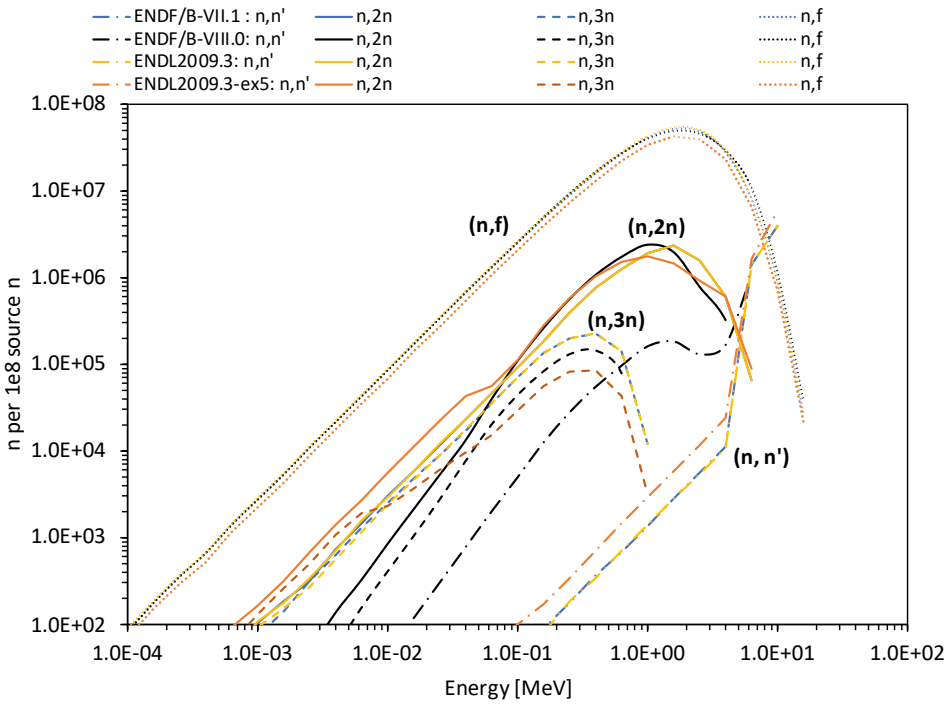

FIG. 15. Simulated energy distribution of outgoing neutrons following a single (n, n') reaction (dot-dashed line), $(n, 2n)$ reaction (full line), $(n, 3n)$ reaction (dashed line) and (n, f) reaction (dotted line) for 14 MeV neutrons incident on ^{241}Am for ENDL2009.3-ex5 (orange). Also shown are the corresponding distributions for ENDF/B-VIII.0 (black), END2009.3 (yellow) and ENDF/B-VII.1 (blue).

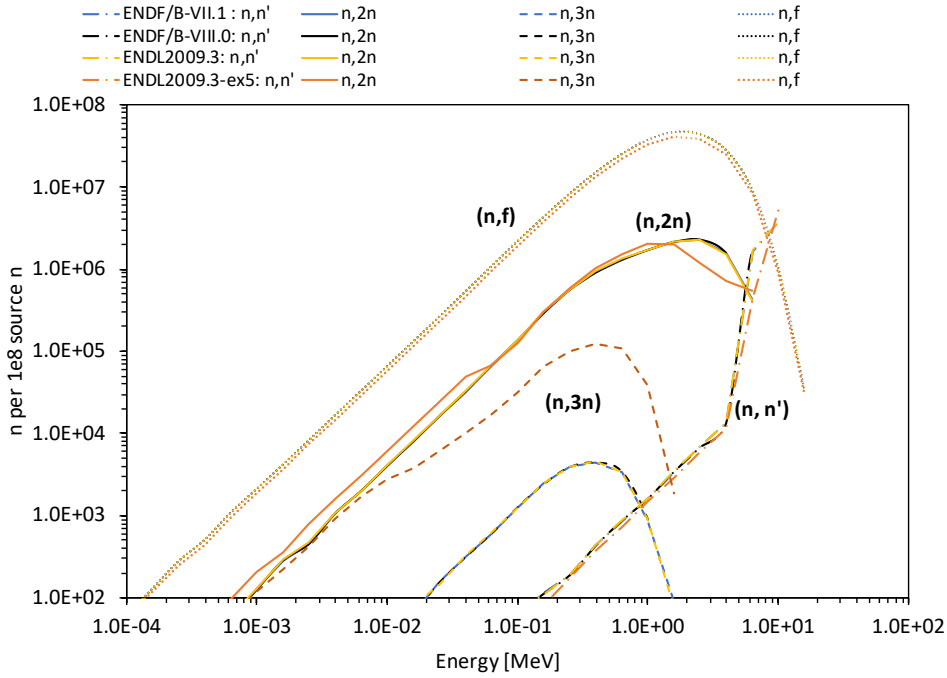

FIG. 16. Simulated energy distribution of outgoing neutrons following a single (n, n') reaction (dot-dashed line), $(n, 2n)$ reaction (full line), $(n, 3n)$ reaction (dashed line) and (n, f) reaction (dotted line) for 14 MeV neutrons incident on ^{242}Am for ENDL2009.3-ex5 (orange). Also shown are the corresponding distributions for ENDF/B-VIII.0 (black), END2009.3 (yellow) and ENDF/B-VII.1 (blue).

TABLE VI. C/E for ^{241}Am(n,γ) and ^{241}Am(n,f) reaction ratios in benchmark critical assemblies. Mercury calculations were run with ENDF/B-VII.1, ENDF/B-VIII.0, ENDL2009.3, and ENDL2009.3-ex5. The (n,γ) reaction ratios account for the isomeric ratio of fast neutron capture and the fraction of ^{242g}Am that beta decays to ^{242}Cm is taken into account.

Reaction Ratio	ICSBEP Critical Assembly	ENDF/B-VII.1. 7 C/E	ENDF/B-VIII.0 C/E	ENDL2009.3 C/E	ENDL2009.3-ex5 C/E
^{241}Am$(n,\gamma)/^{235}$U(n,f)	PU-MET-FAST-006 (Flattop Pu)	0.817	0.863	0.843	0.855
^{241}Am$(n,\gamma)/^{235}$U(n,f)	IEU-MET-FAST-007 (Bigten)	0.774	0.782	0.818	0.807
^{241}Am$(n,\gamma)/^{235}$U(n,f)	FUND-IPPE-FR-MULT-RRR-001	-	0.947	0.954	0.969

The angular and energy distributions of outgoing neutrons after a single interaction simulated with the ENDL2009.3-ex5, ENDL2009.3, ENDF/b-VII.1 and ENDF/b-VIII.0 cross section libraries are shown in Figures 11 - 13. These are typical examples of V&V results that can provide feedback on specific evaluations. These results show a slightly smaller (n,f) and larger $(n,3n)$ cross-sections at 14 MeV in the new ^{240}Am and ^{242}Am evaluations. Simulations results for ENDF/B-VIII.0 ^{241}Am(n,n') neutron exit distribution are consistent with the evaluated data.

Validation of the new ^{241}Amevaluation described in this report relies on integral benchmark activation experiments since, to the best of our knowledge, there are no criticality benchmarks available for ^{240,241,242}Am [16]. ^{241}Amfoils were irradiated at the center of several fast critical assemblies to determine reaction rates for ^{241}Am(n,γ) and ^{241}Am(n,f) . The published data and simulated results are given in terms of reaction ratios, where the reaction rate of interest is normalized by ^{235}U(n,f) or ^{239}Pu(n,f). ^{241}Amreaction rates calculated with Mercury (C) are compared to benchmark experiments (E) and C/E are presented in Table VI. While Mercury calculations of capture reaction ratios are consistent across libraries, they are about 20% lower than the experimental benchmarks. It is perhaps related to the implementation of ^{241}Am$(n,\gamma)^{242g}$Am yield and to the fraction of ^{242g}Am that beta decays to ^{242}Cm. Finally, the fission ratio for the new ^{241}Amevaluation is in good agreement with the FUND-IPPE-FR-MULT-RRR-001 benchmark and with published C/E for ^{241}Am$(n,f)/^{235}$U(n,f) calculated with MCNP6 and ENDF/B libraries. CMCNP6/E was 0.947 for ENDF/B-VII.1 and 0.943 for ENDF/B-VIII.0 [6, 17].

A. Internal library release

Following the V&V tests, the new recommended 'experimental' library ENDL2009.3-ex5, including the new evaluations of the ^{240}Am, ^{241}Am and ^{242}Am cross sections, was released for internal use within LLNL.

VII. CONCLUSIONS

We have performed a new data evaluation of ^{240}Am, ^{241}Am and ^{242}Am cross sections using newly obtained fission cross section data. The new evaluations (ENDL2009.3-ex5) include the nuclear cross sections for (n,γ), $(n.n')$, $(n,2n)$, $(n,3n)$, (n,f), and all their associated distributions. The evaluations were then translated into ENDL format via GNDS using a new parser, and processed into accessible libraries for Monte Carlo and Deterministic simulation codes WITH MCFGEN and NDFGEN, respectively. The ENDL2009.3-ex5mcf Monte Carlo library was then used for a simulation on a "broomstick" example to verify the integrity of the library and check the functionality of the results. The ENDL2009.3-ex5mcf library has now been released as an "experimental" version for internal access. All results have been documented within this report, through the associated references and the appendices at the end of this report.

VIII. ACKNOWLEDGMENTS

This work was funded by the Office of Defense Nuclear Nonproliferation Research and Development within the U.S. Department of Energy's National Nuclear Security Administration by Lawrence Livermore National Laboratory

under Contract No DE-AC52-07NA27344.

---

[1] R. J. Casperson, J. T. Burke, N. D. Scielzo, J. E. Escher, E. McCleskey, M. McCleskey, A. Saastamoinen, A. Spiridon, A. Ratkiewicz, A. Blanc, M. Kurokawa, and R. G. Pizzone, Phys. Rev. C **90**, 034601

[2] H. C. Britt and J. B. Wilhelmy, J. Nucl. Sci. and Eng. **72**, 222 (1979).

[3] W. E. Ormand, private communication.

[4] I. J. Thompson, Computer Physics Reports **7**, 167 (1988); I. J. Thompson, FRESCO manual, http://www.fresco.org.uk/.

[5] E. Sh. Soukhovitskii, S. Chiba, J.-Y. Lee, O. Iwamoto and T. Fukahori, J. Phys. G: Nucl. Part. Phys. **30**, 905 (2004); E. Sh. Soukhovitskii, R. Capote, J. M. Quesada, S. Chiba, and D. S. Martyanov, Phys. Rev. C **94**, 064605 (2016).

[6] M. B. Chadwick *et al.*, Nuclear Data Sheets **112**, 2887 (2011).

[7] A. J. Koning and M. C. Duijvestijn, Nucl. Phys. **A744**, 15 (2004).

[8] M. Baba, H. Wakabayashi, K. Maeda, and N. Hirakawa, J. Nucl. Sci. and Tech. **27**, 601 (1990).

[9] R. Vogt, private communication.

[10] A. J. Koning, S. Hilaire, and S. Goriely, TALYS-1.8, *A nuclear reaction program*, User manual, www.talys.eu

[11] J. Kopecky and M. Uhl, Phys. Rev. C **41**, 1941 (1990).

[12] P. Vranas et a., LLNL-SM-733021 (2017)

[13] "Mercury" web site, accessed: 2017-09-22. [Online]. Available: https://wci.llnl.gov/simulation/computer-codes/mercury

[14] P. S. Brantley et al., Mercury User Guide: Version d.8, LLNL-SM-560687, Lawrence Livermore National Laboratory (2012).

[15] I. J. Thompson, *et al.*, Technical report, LlNL-TR-741270 (2017)

[16] International Criticality Safety Benchmark Evaluation Project (ISCBEP), International Handbook of Evaluated Criticality Safety Benchmark Experiments, NEA/NSC/DOC/(95)03, September 2011 Edition [CD-ROM], Nuclear Energy Agency (2011).

[17] D.A. Brown, et al., Nucl. Data Sheets, 148, 1 (2018).